Efficient bulk-heterojunction photovoltaic cells with transparent multi-layer graphene electrodes

Minhyeok Choe [a,1], Byoung Hoon Lee [a,1], Gunho Jo [a], June Park [c], Woojin Park [a], Sangchul Lee [b], Woong-Ki Hong [a,2], Maeng-Je Seong [c], Yung Ho Kahng [a], Kwanghee Lee [a,b,*], Takhee Lee [a,b,**]

[a] Department of Materials Science and Engineering, Gwangju Institute of Science and Technology, Gwangju 500-712, Republic of Korea
[b] Department of Nanobio Materials and Electronics, Gwangju Institute of Science and Technology, Gwangju 500-712, Republic of Korea
[c] Department of Physics, Chung-Ang University, Seoul 156-756, Republic of Korea

ABSTRACT

We present the results of applying multi-layer graphene (MLG) films as transparent conductive electrodes in organic photovoltaic devices (OPVs). The MLG films synthesized at different growth temperatures by chemical vapor deposition were applied to OPVs. The performance of OPVs with 1000 °C-grown MLG films was found to be the best with a power conversion efficiency (PCE) of ~1.3%. The PCE was further enhanced when a hole-blocking TiO_X layer was inserted in the device structure, resulting in a PCE of ~2.6% which is a significantly higher efficiency compared to other previously reported graphene-adopted photovoltaic cells. Our demonstration of the PCE-increase in the graphene-electrode OPVs may foster the application of the fast-progressing graphene technology toward more practical OPV technology.

1. Introduction

Graphene, a two-dimensional sheet of covalently bonded carbon atoms, has been attracting great attention in the field of optoelectronics of organic and inorganic materials. This is because of its outstanding electronic, optical, and mechanical properties, such as quantum electronic transport properties, transparency, mechanical and chemical stability, stretchability, and flexibility [1–6]. Currently, graphene films that can be deposited on arbitrary substrates are prepared by various techniques, including

* Corresponding author at: Department of Materials Science and Engineering, Gwangju Institute of Science and Technology, Gwangju 500-712, Republic of Korea. Tel.: +82 62 715 2325; fax: +82 62 715 2304.
** Corresponding author at: Department of Materials Science and Engineering, Gwangju Institute of Science and Technology, Gwangju 500-712, Republic of Korea. Tel.: +82 62 715 2313; fax: +82 62 715 2304.
E-mail addresses: klee@gist.ac.kr (K. Lee), tlee@gist.ac.kr (T. Lee).
[1] These authors contributed equally to this work.
[2] Present address: Nanoscience Centre, University of Cambridge, Cambridge CB3 0FF, UK.

mechanical exfoliation of graphite crystals, reduction of graphene oxide films, and growth by chemical vapor deposition (CVD) [6–11]. In this study, we used the CVD method for graphene production. This method offers several advantages, including the capability to grow large and continuous uniform films with low sheet resistances, transferability to arbitrary substrates, and controllability of the synthesized film properties. It has been reported that the graphene films produced by CVD typically have sheet resistances of 300–1000 $\Omega/\square$ and mobilities of 300–4000 cm^2/V s [4,8,9].

In this work, our focus is on the application of graphene films as the electrodes in organic photovoltaic cells. In the optoelectronics, the need for a noble material to replace indium tin oxide (ITO) that can be produced cheaply while providing high transparency and conductivity has emerged [12,13]. Graphene films potentially fulfill all of these required properties and are therefore currently being vigorously researched [4,5,10,11,14–23]. Wang et al. [11] first reported the application of graphene films in dye-sensitized photovoltaic cells and obtained a power conversion efficiency (PCE) of 0.26%. A number of reports followed.

Tung et al. [5] reported organic bulk-heterojunction (BHJ) photovoltaic cells with modified graphene films composited with carbon nanotubes and demonstrated a 0.85% PCE. More recently, Wang et al. [14] used functionalized graphene films in organic BHJ photovoltaic cells and reported an improved PCE of 1.71%. Overall, BHJ photovoltaic cells with graphene electrodes have exhibited PCEs below 2% to date [5,11,14–17]. These PCEs are only proof-of-concept and are far below the best performance obtained from organic solar cells made with ITO electrodes. Values of 6.1% [24], with a BHJ structure, and 6.5% [25], with a tandem cells structure, have both been reported by the research group of Heeger and Lee, one of co-authors of this paper. Recently, a PCE of 6.7% has been reported from an organic BHJ structure with low bandgap polymers having an enhanced open-circuit voltage [26,27]. On the contrary, the poor performance of photovoltaic cells incorporating graphene electrodes is apparently due to the poor quality of graphene films: high sheet resistances and interfacing problems with the active layers.

In this paper, we report an application of CVD-synthesized multi-layer graphene (MLG) films incorporated as transparent and conductive electrodes of organic BHJ photovoltaic cells (OPVs). Particularly, the growth temperature of the graphene films was studied as a control parameter on the PCE of the graphene-OPVs. Overall, the MLG films showed good performance as electrodes for OPVs, and among tested graphene-OPVs the 1000 °C-grown MLG films were found to yield the best PCE. Furthermore, when a thin sol–gel processed titanium sub-oxide (TiO_X) layer was inserted in the cell, the PCE was further increased to ~2.60%. Our results show the control of the graphene film quality and the cell structure optimization with a TiO_X layer can increase the performance of OPVs beyond the proof-of-concept level.

2. Experimental

The device structure of a photovoltaic cell with graphene as a transparent and conducting electrode is shown in Fig. 1(a). To synthesize graphene films, 300 nm thick Ni-deposited substrates were placed into the CVD chamber and heated to 800, 900, or 1000 °C under the flow of a 4% H_2 in Ar gas mixture. Then, a graphene film was grown by adding CH_4 gas to the flow. After growth, the substrate was rapidly cooled to room temperature (>200 °C/min initially and slower later) to suppress excessive precipitation of carbon atoms. Finally, the graphene film was released from the Ni substrate by etching Ni in an aqueous solution of iron chloride ($FeCl_3$) [4]. The CVD-synthesized MLG film was transferred onto a glass substrate to form the anode for OPV. Before a poly(3,4-ethylenedioxythiophene) poly(styrenesulfonate) (PEDOT:PSS) layer was spin coated on top of the graphene film, the graphene film was undergone an ozone treatment to produce the hydrophilic surface, which was a necessary step to increase the coating efficiency of PEDOT:PSS on graphene. Next, the photoactive BHJ composite of poly(3-hexylthiophene) (P3HT) and [6,6]-phenyl-C61 butyric acid methyl ester (PCBM) was spin coated on top of the PEDOT:PSS layer. Then, a TiO_X film was spin coated for some devices. Finally, aluminum was thermally evaporated to form the cathode. A cross-sectional high-resolution transmission electron microscopy (HRTEM) image of a prepared photovoltaic cell (Fig. 1(b)) clearly shows that the individual layers were nicely formed with distinctive interfaces; the TiO_X film and MLG film are shown in the upper and lower inset of Fig. 1(b), respectively.

3. Results and discussion

3.1. Characteristics of multi-layer graphene films

Before applying the MLG films in photovoltaic cells, we investigated the properties of these films using various techniques. To determine the morphological features and thicknesses of the MLG films, we used an atomic force microscope (AFM) to image a transferred MLG film on a 300-nm-thick SiO_2 layer on a Si substrate, as shown in Fig 2(a). The thinnest part measured on our graphene film is 1.13 nm, as shown in the cross-sectional profile in Fig. 2(b). This thickness corresponds to the thickness of a monolayer; due to the chemical contrast between graphene and substrate, the monolayer thickness has been measured as ~1 nm by AFM [7,9,28–30]. Fig. 2(c) shows the TEM images for a graphene film. Our graphene films consisted of mono to multi-layer regions and contained rippled regions, as marked by a square in the lower image. By counting the number and the distance of the bright and dark stripes in the rippled region, the number of
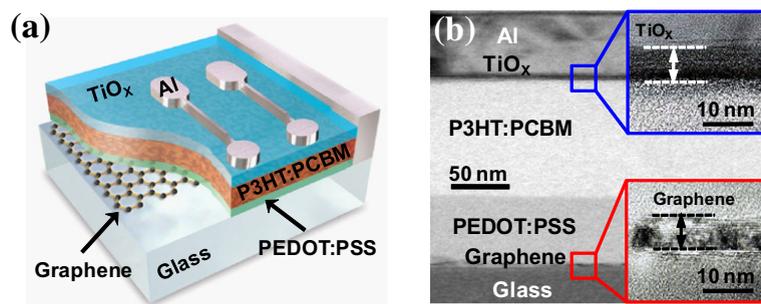
Fig. 1. (a) Schematic diagram of the photovoltaic device structure with MLG electrodes and a hole-blocking TiO_X layer. (b) TEM cross-sectional image of a photovoltaic device. The insets show HRTEM images near the TiO_X layer (top) and near the MLG films (bottom).
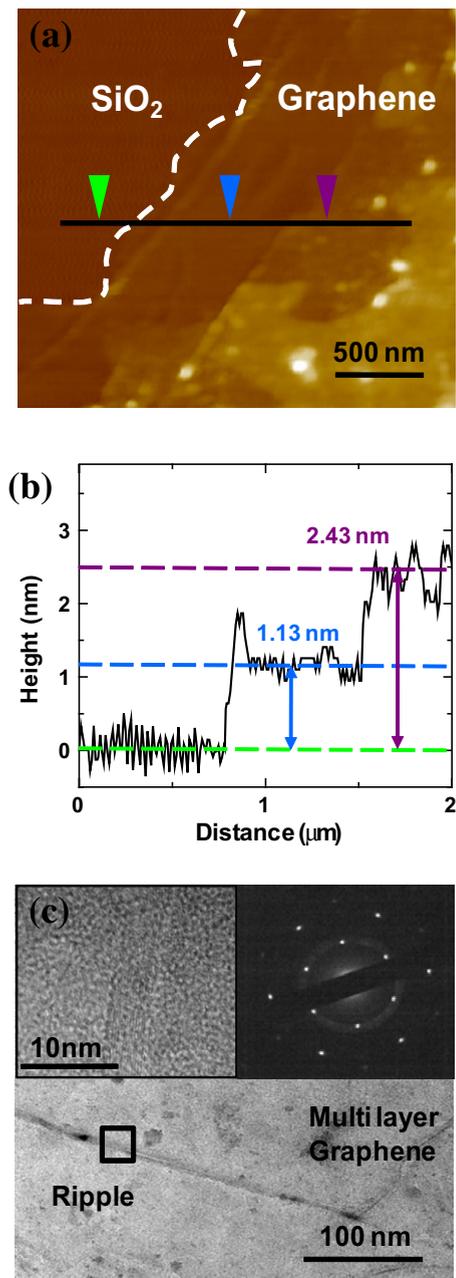
Fig. 2. (a) AFM image of a MLG film showing the edge of the MLG layers (dashed) on a SiO$_2$ substrate. (b) Topographic height profiles across the solid line indicated in (a). (c) TEM image of a region of MLG. The insets show an HRTEM image of the rippled region (top left) and an electron diffraction pattern (top right) of MLG.

graphene layers (~15) and the interlayer distance (3.5 ± 0.1 Å) were obtained; the results were found consistent with values reported previously [9,31]. The electron diffraction (ED) pattern (upper right inset, Fig. 2(c)) taken on a monolayer region shows a hexagonal spot pattern, confirming the threefold symmetry of the arrangement of carbon atoms in the graphene film.

Raman spectroscopy using the 514 nm line of an Ar+ laser was used to analyze the properties of MLG films

grown at three different temperatures (Fig. 3). Raman spectroscopy is a non-destructive analysis tool which provides high-throughput and unambiguous identification of the properties of graphene films with three most intense peaks: D peak at ~1350 cm^{-1}, G peak at ~1580 cm^{-1}, and 2D peak at ~2700 cm^{-1} [32–34]. Our CVD-grown graphene films typically showed multi-layer-type Raman features (i.e., G-peak intensity > 2D-peak intensity) and small D peaks that were related to defects on MLG. The integrated intensity ratios of the observed Raman peaks are shown in Fig. 3(b) and (c). The ratios of the G-peak intensity to the 2D-peak intensity (I_G/I_{2D}) shown in Fig 3(b) indicate that the average thickness of the graphene film increased as the growth temperature increased since the higher ratio corresponds to the thicker graphene film. The ratios of the D-peak intensity to the G-peak intensity (I_D/I_G) shown in Fig. 3(c) correspond with the average density of defects [33–35], and these ratios indicate that the defect density decreased as the growth temperature increased. From the comparison of Raman peak ratios, we conclude that the growth temperature significantly affects the properties of the graphene in terms of the film thickness and defect density.

Furthermore, the film property that is directly relevant to the performance of the organic photovoltaics was investigated: the optical transmittances and the sheet resistances of the MLG films synthesized at three different growth temperatures. Results are summarized in Fig. 4. Fig. 4(a) shows the representative transmittances of MLG films prepared at different growth temperatures and the inset shows the transmittance of 90.7 ± 1.5, 88.8 ± 2.2, and 86.9 ± 1.2% at 515 nm wavelength according to the growth temperatures of 800, 900, and 1000 °C, respectively. The plot of mobility versus resistance, shown in Fig. 4(b), was obtained by taking the statistical means and standard deviations of 8–10 synthesized-MLG films at each growth temperature. As expected from Raman analysis, higher temperature grown thicker MLG films yielded less transparency and lower sheet resistance. Specifically, MLG films prepared at growth temperatures of 800, 900, and 1000 °C showed the sheet resistances of 1730 ± 600, 990 ± 400, and 610 ± 140 Ω/□, and the mobility of 660 ± 270, 1030 ± 440, and 1180 ± 260 cm^2/V s respectively. Furthermore, we measured the work function of the MLG films by using a Kelvin probe measurement system. As shown in Fig. S2(b) in Supplementary material, the work function of the graphene films was 4.45 ± 0.04 eV and did not change significantly with the growth temperature change.

3.2. Performance of the organic photovoltaic cells with graphene electrode

Fig. 5(a) shows the representative current density–voltage (J–V) data of the fabricated OPVs without TiO$_x$ layers under AM 1.5 G irradiation by a solar simulator with an irradiation intensity of 100 mW/cm^2. The three different MLG films prepared at different growth temperatures (800, 900, and 1000 °C) were used to compare the performance as electrodes in OPVs. The best performance was achieved from the devices using MLG films that were
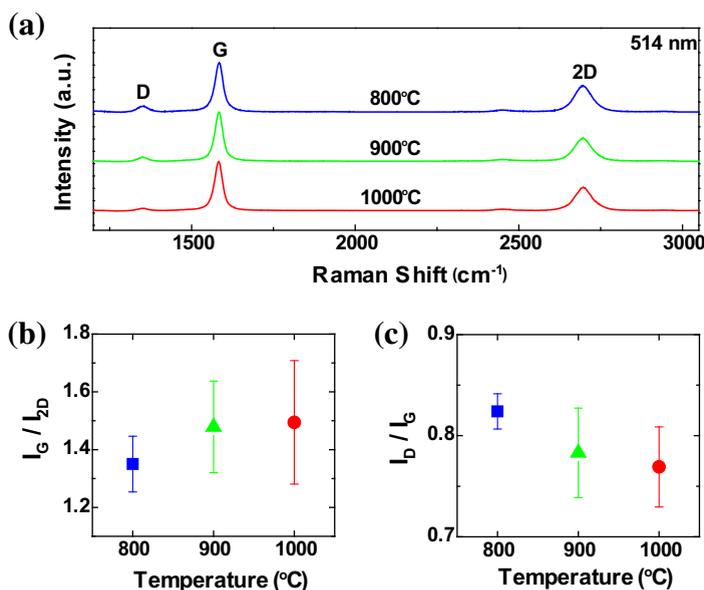
Fig. 3. (a) Raman spectra of MLG films synthesized at different growth temperatures (800, 900, and 1000 °C). (b) Integrated intensity ratios of G peak and 2D peak (I_G/I_{2D}), and (c) of D peak and G peak (I_D/I_G) as a function of growth temperature. These integrated intensity peaks are from the Raman spectra of graphene films.
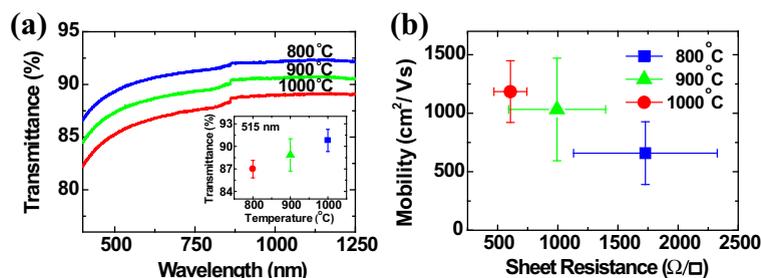
Fig. 4. (a) Transmission spectra of MLG films. The inset shows the transmittance of 90.7 ± 1.5, 88.8 ± 2.2, and 86.9 ± 1.2% at 515 nm wavelength, 800, 900, and 1000 °C, respectively. (b) Mobility versus sheet resistance of MLG films prepared at different growth temperatures (800, 900, and 1000 °C).
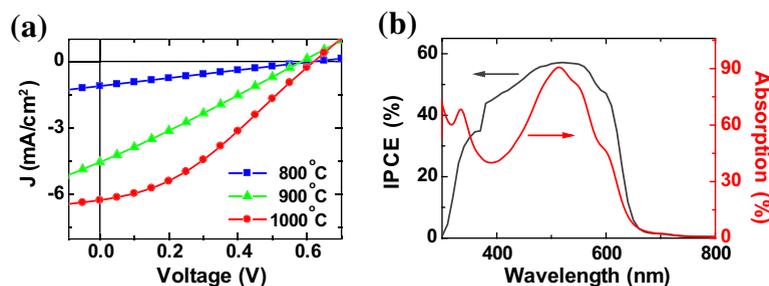
Fig. 5. (a) J-V curves of photovoltaic cells with MLG films grown at different growth temperatures under AM 1.5 G irradiation conditions. (b) Incident photon-to-current efficiency (IPCE) and absorption spectra of a photovoltaic device fabricated with a 1000 °C-grown MLG film.

prepared at 1000 °C. Specifically, for the case of the 1000 °C-graphene OPV, the representative parameters obtained were short-circuit current density (J_{SC}) of 6.25 mA/cm^2, open-circuit voltage (V_{OC}) of 0.62 V, and fill factor (FF) of 0.35. These values yielded PCE = $J_{SC}V_{OC}$FF/P_{inc} (here P_{inc} is the intensity of incident light) of 1.34%. The parameters for the devices with graphene films prepared at 800 and 900 °C are summarized in Table 1. Fig. 5(b) compares

Table 1

Summary of the performance parameters of graphene-electrode organic photovoltaic devices fabricated with graphene films that were synthesized at different growth temperatures (800, 900, and 1000 °C) and ITO-electrode devices. Short-circuit current density (J_{SC}), open-circuit voltage (V_{OC}), fill factor (FF), and power conversion efficiency (PCE) are listed. The improvement of the performance parameters by the insertion of the TiO_X layer as a hole-blocking layer (HBL) was compared in all the device types.

Temp. (°C)	HBL	V_{OC} (V)	J_{SC} (mA/cm²)	FF	PCE (%)
800	–	0.62	1.11	0.25	0.17
800	TiO_X	0.59	6.45	0.32	1.22
900	–	0.59	4.54	0.26	0.70
900	TiO_X	0.62	7.57	0.46	2.13
1000	–	0.62	6.25	0.35	1.34
1000	TiO_X	0.60	9.03	0.48	2.60
ITO	–	0.63	7.50	0.50	2.34
ITO	TiO_X	0.63	9.02	0.67	3.80

the incident photon-to-current collection efficiency (IPCE) spectrum and absorption spectrum of a device fabricated using MLG films prepared at 1000 °C. The graphene-electrode photovoltaic cell without a TiO_X layer showed the typical spectral response of P3HT:PCBM composites with a maximum IPCE of approximately 57% at 515 nm.

The performance of the graphene photovoltaic devices was further enhanced when a TiO_X film was added between the aluminum cathode and the photo-active layer. Fig. 6(a) compares the *J–V* curves of the photovoltaic devices with 1000 °C-grown MLG electrodes and with ITO electrodes with and without the TiO_X layer. The performance parameters obtained from the MLG-electrode devices with the TiO_X layer shown in this figure are J_{SC} of 9.03 mA/cm², V_{OC} of 0.60 V, and FF, which was dramatically increased, of 0.48. The corresponding PCE was significantly increased to 2.60%. Such performance enhancement by adding a TiO_X film was also observed in photovoltaic cells with ITO electrodes. The representative parameters obtained for the case of the ITO-electrode devices with the TiO_X layer were J_{SC} of 9.02 mA/cm², V_{OC} of 0.63 V, and FF of 0.67, and the PCE was determined as 3.80%. The enhancement of PCE for our graphene-electrode and ITO-electrode photovoltaic devices by inserting a TiO_X layer can be explained by the role of the TiO_X layer that creates a higher density of photo-generated charge carriers as an

optical spacer [36,37] and facilitates better transport of charge carriers to each electrode as a hole-blocking layer [24,25,38,39], thereby increasing J_{SC}. Recently, Roy et al. [37] have compared the calculated and the experimentally measured total absorption spectra of photovoltaic devices with and without the TiO_X layer and confirmed the effect of the TiO_X layer as an optical spacer. Also, Cho et al. [38] have demonstrated the hole-blocking property of TiO_X using multilayer bipolar field-effect transistors (FETs). In their device, the TiO_X layer was inserted to separate the n-channel material and the p-channel material. Because the TiO_X layer retained the injected holes within the p-channel material and transferred the injected electrons into the n-channel material, their device successfully showed the J–V characteristics. As a result, the PCE of our photovoltaic devices with TiO_X was improved by the effects of the TiO_X layer both as an optical spacer and as a hole-blocking layer. Moreover, the TiO_X layer reduced the contact resistance between the aluminum cathode and the P3HT:PCBM photo-active layer, consequently increasing the FF in the device. Fig. 6(b) presents detailed statistical data for PCE values that were statistically determined from all the measured graphene-electrode devices in comparison with the ITO-electrode devices, with and without the TiO_X layers. Each statistical value in Fig. 6(b) was extracted from all the measured devices shown in the Supplementary material (Fig. S1). For devices without the TiO_X layer, the PCEs (the mean and standard deviation) of the photovoltaic devices were determined as 0.19 ± 0.08, 0.56 ± 0.10, and 1.38 ± 0.35% with the graphene-electrodes grown at 800, 900, and 1000 °C, respectively, in comparison to 1.20 ± 0.27, 1.79 ± 0.31, and 2.58 ± 0.45% for the devices with TiO_X layer and the graphene-electrodes grown at 800, 900, and 1000 °C, respectively. Also, we found that the PCE of the ITO-electrode photovoltaic devices without TiO_X was 2.53 ± 0.42% compared to 3.74 ± 0.31% of those with TiO_X. It can be noticed that the PCEs for ITO-electrode devices were higher than those for graphene-electrode devices, partly due to higher conductivity of ITO film than that of graphene films. Furthermore, the best PCE observed was 3.63% from a 1000 °C-grown graphene-electrode device with the TiO_X layer. However, this value was outside of the one sigma criterion, i.e., the 3.63% value was beyond
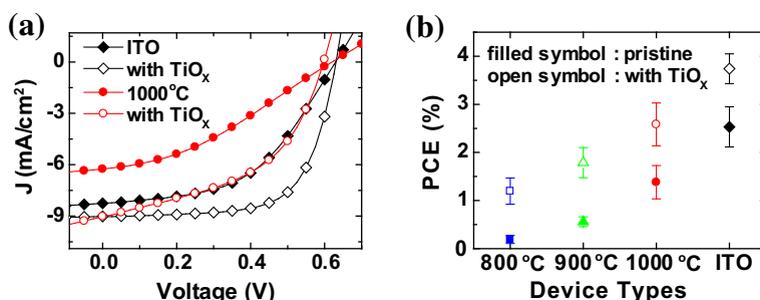
Fig. 6. (a) *J–V* curves of photovoltaic devices with 1000 °C-grown MLG electrodes (circles) and with ITO electrodes (diamonds). The curves without the TiO_X layer (filled symbols) are compared to the ones with the TiO_X layer (open symbols). (b) The PCEs for graphene-electrode photovoltaic devices in comparison with those for the ITO-electrode photovoltaic devices with the TiO_X layers and without the TiO_X layers (pristine). This statistical means and standard deviations were extracted from Supplementary material. The types of the devices are indicated on the x-axis (800, 900, and 1000 °C: graphene-electrode devices, ITO: ITO-electrode devices).

one $\sigma = 0.45\%$ (standard deviation) from the mean of $m = 2.58\%$. The performance parameters for all types of photovoltaic devices measured in this study are summarized in Table 1. Although our results indicate that the efficiency of OPVs can be significantly enhanced by graphene film quality control and by inserting a TiO_X layer, there are rooms for improvements to compete with the efficiency of ITO-electrode OPVs. With more research to further enhance the graphene film quality and to further optimize the device structure, graphene films may soon be widely used as an alternative material to ITO films in organic photovoltaics.

4. Conclusions

In summary, we reported the application of MLG films grown by chemical vapor deposition to organic photovoltaic cells. The effect of graphene synthesis temperature on the performance as anode in OPVs was studied. The 1000 °C-grown MLG films, that possessed sheet resistances of ∼606 Ω/□ at transmittances of ∼87%, showed the best performance as electrodes in OPVs. Furthermore, a cell structure optimization with an inserted TiO_X layer enhanced the observed power conversion efficiency up to 2.58 ± 0.45%. Our demonstration of efficiency improvements in graphene-adopted photovoltaic cells may foster the application of fast-progressing graphene technology into the practical realm of organic photovoltaic cells.

Acknowledgements

Appendix A. Supplementary material

Supplementary data associated with this article can be found, in the online version, at doi:10.1016/j.orgel.2010.08.018.

References

[1] K.S. Novoselov, A.K. Geim, S.V. Morozov, D. Jiang, M.I. Katsnelson, I.V. Grigorieva, S.V. Dubonos, A.A. Firsov, Nature 438 (2005) 197.
[2] X. Du, I. Skachko, A. Barker, E.Y. Andrei, Nat. Nanotechnol. 3 (2008) 491.
[3] D.V. Kosynkin, A.L. Higginbotham, A. Sinitskii, J.R. Lomeda, A. Dimiev, B.K. Price, J.M. Tour, Nature 458 (2009) 872.
[4] K.S. Kim, Y. Zhao, H. Jang, S.Y. Lee, J.M. Kim, K.S. Kim, J.-H. Ahn, P. Kim, J.-Y. Choi, B.H. Hong, Nature 457 (2009) 706.
[5] V.C. Tung, L.-M. Chen, M.J. Allen, J.K. Wassei, K. Nelson, R.B. Kaner, Y. Yang, Nano Lett. 9 (2009) 1949.
[6] H.A. Becerril, J. Mao, Z. Liu, R.M. Stoltenberg, Z. Bao, Y. Chen, ACS Nano. 2 (2008) 463.
[7] K.S. Novoselov, A.K. Geim, S.V. Morozov, D. Jiang, Y. Zhang, S.V. Dubonos, I.V. Grigorieva, A.A. Firsov, Science 306 (2004) 666.
[8] X. Li, W. Cai, J. An, S. Kim, J. Nah, D. Yang, R. Piner, A. Velamakanni, I. Jung, E. Tutuc, S.K. Banerjee, L. Colombo, R.S. Ruoff, Science 324 (2009) 1312.
[9] A. Reina, X. Jia, J. Ho, D. Nezich, H. Son, V. Bulovic, M.S. Dresselhaus, J. Kong, Nano Lett. 9 (2009) 30.
[10] G. Jo, M. Choe, C.-Y. Cho, J.H. Kim, W. Park, S. Lee, W.-K. Hong, T.-W. Kim, S.-J. Park, B.H. Hong, Y.H. Kahng, T. Lee, Nanotechnology 21 (2010) 175201.
[11] X. Wang, L. Zhi, K. Mullen, Nano Lett. 8 (2008) 323.
[12] S.K. Hau, H.-L. Yip, J. Zou, A.K.Y. Jen, Org. Electron. 10 (2009) 1401.
[13] R.C. Tenent, T.M. Barnes, J.D. Bergeson, A.J. Ferguson, B. To, L.M. Gedvilas, M.J. Heben, J.L. Blackburn, Adv. Mater. 21 (2009) 3210.
[14] Y. Wang, X. Chen, Y. Zhong, F. Zhu, K.P. Loh, Appl. Phys. Lett. 95 (2009) 063302.
[15] G. Eda, Y.-Y. Lin, S. Miller, C.-W. Chen, W.-F. Su, M. Chhowalla, Appl. Phys. Lett. 92 (2008) 233305.
[16] J. Wu, H.A. Becerril, Z. Bao, Z. Liu, Y. Chen, P. Peumans, Appl. Phys. Lett. 92 (2008) 263302.
[17] X. Wang, L. Zhi, N. Tsao, Z. Tomovic, J. Li, K. Mullen, Angew. Chem. Int. Ed. 47 (2008) 2990.
[18] J. Wu, M. Agrawal, H.A. Becerril, Z. Bao, Z. Liu, Y. Chen, P. Peumans, ACS Nano. 4 (2010) 43.
[19] Z. Yin, S. Wu, X. Zhou, X. Huang, Q. Zhang, F. Boey, H. Zhang, Small 6 (2010) 307.
[20] P. Blake, P.D. Brimicombe, R.R. Nair, T.J. Booth, D. Jiang, F. Schedin, L.A. Ponomarenko, S.V. Morozov, H.F. Gleeson, E.W. Hill, A.K. Geim, K.S. Novoselov, Nano Lett. 8 (2008) 1704.
[21] N. Yang, J. Zhai, D. Wang, Y. Chen, L. Jiang, ACS Nano. 4 (2010) 887.
[22] S. Sun, L. Gao, Y. Liu, Appl. Phys. Lett. 96 (2010) 083113.
[23] S. Bae, H. Kim, Y. Lee, X. Xu, J.-S. Park, Y. Zheng, J. Balakrishnan, T. Lei, H.R. Kim, Y.I. Song, Y.-J. Kim, K.S. Kim, B. Özyilmaz, J.-H. Ahn, B.H. Hong, S. Iijima, Nat. Nanotechnol. 5 (2010) 574.
[24] S.H. Park, A. Roy, S. Beaupre, S. Cho, N. Coates, J.S. Moon, D. Moses, M. Leclerc, K. Lee, A.J. Heeger, Nat. Photonics 3 (2009) 297.
[25] J.Y. Kim, K. Lee, N.E. Coates, D. Moses, T.-Q. Nguyen, M. Dante, A.J. Heeger, Science 317 (2007) 222.
[26] J. Hou, H.-Y. Chen, S. Zhang, R.I. Chen, Y. Yang, Y. Wu, G. Li, J. Am. Chem. Soc. 131 (2009) 15586.
[27] H.-Y. Chen, J. Hou, S. Zhang, Y. Liang, G. Yang, Y. Yang, L. Yu, Y. Wu, G. Li, Nat. Photonics 3 (2009) 649.
[28] C. Gomez-Navarro, R.T. Weitz, A.M. Bittner, M. Scolari, A. Mews, M. Burghard, K. Kern, Nano Lett. 7 (2007) 3499.
[29] S. Gilje, S. Han, M. Wang, K.L. Wang, R.B. Kaner, Nano Lett. 7 (2007) 3394.
[30] M.J. Allen, V.C. Tung, L. Gomez, Z. Xu, L.-M. Chen, K.S. Nelson, C. Zhou, R.B. Kaner, Y. Yang, Adv. Mater. 21 (2009) 2098.
[31] X. Wang, H. You, F. Liu, M. Li, L. Wan, S. Li, Q. Li, Y. Xu, R. Tian, Z. Yu, D. Xiang, J. Cheng, Chem. Vap. Dep. 15 (2009) 53.
[32] Y.y. Wang, Z.h. Ni, T. Yu, Z.X. Shen, H.m. Wang, Y.h. Wu, W. Chen, A.T.S. Wee, J. Phys. Chem. C 112 (2008) 10637.
[33] A.C. Ferrari, Solid State Commun. 143 (2007) 47.
[34] L.G. Cancado, K. Takai, T. Enoki, M. Endo, Y.A. Kim, H. Mizusaki, A. Jorio, L.N. Coelho, R. Magalhaes-Paniago, M.A. Pimenta, Appl. Phys. Lett. 88 (2006) 163106.
[35] M.J. Matthews, M.A. Pimenta, G. Dresselhaus, M.S. Dresselhaus, M. Endo, Phys. Rev. B 59 (1999) R6585.
[36] J.Y. Kim, S.H. Kim, H.-H. Lee, K. Lee, W. Ma, X. Gong, A.J. Heeger, Adv. Mater. 18 (2006) 572.
[37] A. Roy, S.H. Park, S. Cowan, M.H. Tong, S. Cho, K. Lee, A.J. Heeger, Appl. Phys. Lett. 95 (2009) 013302.
[38] S. Cho, J. Yuen, J.Y. Kim, K. Lee, A.J. Heeger, S. Lee, Appl. Phys. Lett. 92 (2008) 063505.
[39] S. Cho, J.H. Seo, K. Lee, A.J. Heeger, Adv. Funct. Mater. 19 (2009) 1459.